Fluctuation effects and multiscaling of the reaction-diffusion front for A+B to OE

1995 J. Phys. A: Math. Gen. 28 3599

(http://iopscience.iop.org/0305-4470/28/13/007)

J. Phys. A: Math. Gen. 28 (1995) 3599–3621. Printed in the UK

Fluctuation effects and multiscaling of the reaction–diffusion front for $A+B \longrightarrow \emptyset$

Martin Howard† and John Cardy†‡

† Department of Physics, Theoretical Physics, 1 Keble Road, Oxford, OX1 3NP, UK
‡ All Souls College, Oxford, UK

Received 11 January 1995

Abstract. We consider the properties of the diffusion-controlled reaction $A + B \to \emptyset$ in the steady state, where fixed currents of A and B particles are maintained at opposite edges of the system. Using renormalization-group methods, we explicitly calculate the asymptotic forms of the reaction front and particle densities as expansions in $(JD^{-1}|x|^{d+1})^{-1}$, where J are the (equal) applied currents, and D the (equal) diffusion constants. For the asymptotic densities of the minority species, we find, in addition to the expected exponential decay, fluctuation-induced power-law tails, which, for $d < 2$, have a universal form $A|x|^{-\mu}$, where $\mu = 5 + O(\epsilon)$, and $\epsilon = 2 - d$. A related expansion is derived for the reaction rate profile R, where we find the asymptotic power law $R \sim B|x|^{-\mu-2}$. For $d > 2$, we find similar power laws with $\mu = d + 3$, but with non-universal coefficients. Logarithmic corrections occur in $d = 2$. These results imply that, in the time-dependent case, with segregated initial conditions, the moments $\int |x|^q R(x,t)\,dx$ fail to satisfy simple scaling for $q > \mu + 1$. Finally, it is shown that the fluctuation-induced wandering of the position of the reaction front centre may be neglected for large enough systems.

1. Introduction

Since the initial work of Gálfi and Rácz [1], there has been considerable interest in the kinetics of one and two-species annihilation, $A + A \to \emptyset$, and $A + B \to \emptyset$ [1–20, 26–30]. Most analytic and numerical studies have concentrated on the case of either homogeneous initial conditions, or initially entirely segregated reactants. Ben-Naim and Redner [9] were the first to study the case of a steady-state reaction interface, maintained by fixed particle currents imposed at opposite edges of the system. Their equations for the particle densities $a(x,t)$ and $b(x,t)$ were

$$\frac{\partial a}{\partial t} = D\nabla^2 a - \lambda ab \tag{1}$$

$$\frac{\partial b}{\partial t} = D\nabla^2 b - \lambda ab \tag{2}$$

with diffusion constant D, reaction rate constant λ, and with the boundary conditions

$$J = -D\partial_x a|_{x=-L} \qquad 0 = -D\partial_x b|_{x=-L} \qquad 0 = -D\partial_x a|_{x=L} \qquad -J = -D\partial_x b|_{x=L}\,. \tag{3}$$

These equations are asymptotically soluble analytically, giving

$$\begin{Bmatrix} a \\ b \end{Bmatrix} \sim (J/D)|x| \begin{Bmatrix} \theta(-x) \\ \theta(x) \end{Bmatrix} + (\text{constant}) \left(\frac{J^2}{\lambda D}\right)^{1/3} \left(\frac{\lambda J}{D^2}\right)^{-1/12} |x|^{-1/4} e^{-\frac{2}{3}(\lambda J/D^2)^{1/2}|x|^{3/2}} \tag{4}$$

0305-4470/95/133599+23$19.50

where $\theta(x)$ is the Heaviside step function. The relations $w \sim J^{-1/3}$, where w is the reaction front width, and $c \sim J^{2/3}$, where c is the particle concentration in the reaction zone, are also derived in [9]. However, implicit in their formulation is the 'mean-field'-like assumption, $\langle ab \rangle \propto \langle a \rangle \langle b \rangle$, which will no longer be adequate below the critical dimension, due to fluctuations. Cornell and Droz [15] have given an argument for the upper critical dimension of the system (leading to $d_c = 2$), as well as performing numerical simulations. On the basis of these, and mean-field analysis, they have proposed scaling forms for a, b and the reaction front R, which are postulated to be valid both above and below the critical dimension in the scaling limit $w \to \infty$ (or $J \to 0$):

$$R = \frac{J}{w} S\left(\frac{x}{w}\right) \qquad a = \frac{wJ}{D} A\left(\frac{x}{w}\right) \qquad b = \frac{wJ}{D} B\left(\frac{x}{w}\right). \tag{5}$$

In other words, the profiles are characterized by a single length scale w, which itself is suggested in [15] to vary as $w \sim J^{-1/2}$ in $d = 1$, and $w \sim J^{-1/3}$ for $d \geqslant 2$ in the scaling limit. Cardy and Lee [29] have given RG arguments which support this conclusion. However, we defer further discussion, especially with regard to the presence of multiscaling, until section 6.

In this paper, we present the results of the first renormalization-group calculation for the asymptotic properties of the densities and reaction front in the steady state, which systematically takes into account the effect of fluctuations in the stochastic particle dynamics. Previously, the RG had been used to study the late-time behaviour of reactions with homogeneous initial conditions (see [19] and references therein). Our calculational framework will bear considerable similarities with [19]. The basic plan is to map the microscopic dynamics, in the form of a master equation, onto a quantum field theory. This theory is then renormalized (for $d \leqslant 2$) by the introduction of a renormalized coupling, which is shown to have a stable fixed point of order ϵ. We then group the Feynman diagrams into sets whose sums give a particular order of the renormalized coupling constant. It will be demonstrated that this grouping is given by the number of loops. These diagrams may then be evaluated (asymptotically) and the Callan–Symanzik solution used, to obtain perturbative expansions for the densities and reaction front. Note that for $d > 2$ no renormalization is necessary and the diagrams may be evaluated directly.

Although the calculation we present is for the steady state, the same RG methods can also be applied to the time-dependent situation, with initially entirely separated reactants. However, this leads to an analytic calculation of greatly increased complexity, as the quantities involved in the calculation (including the Green functions, the response functions, and the mean-field reaction front) will acquire additional time dependence. Nevertheless we shall argue in section 6 that our results are still valid for the *quasistatic* time-dependent situation, provided we substitute $J \sim t^{-1/2}$.

We now present our results for the asymptotic forms of the densities and reaction front profile. It will be shown that at zero loops we find a stretched exponential dependence which we include in the following summary, even though we expect its effects to be overwhelmed by leading and subleading power-law terms. In addition, for $d < 2$, we do not rule out the possibility of logarithms in higher-order terms summing to give a modification to the leading power law given below (which results from the straightforward evaluation of the one-loop contributions). So we find asymptotically as $|x| \to \infty$ for $d < 2$:

$$\begin{Bmatrix} \langle a \rangle \\ \langle b \rangle \end{Bmatrix} = (J/D)|x| \begin{Bmatrix} \theta(-x) \\ \theta(x) \end{Bmatrix} + A_1 |x|^{(7-5d)/12} \mathrm{e}^{-A_2|x|^{(d+1)/2}} + A_3 |x|^{-5+2\epsilon} + \cdots \tag{6}$$

$$R = \lambda \langle ab \rangle = A_4 |x|^{(7d-5)/12} \mathrm{e}^{-A_2|x|^{(d+1)/2}} + A_5 |x|^{-7+2\epsilon} + \cdots \tag{7}$$

where

$$A_1 = 0.3787\frac{(J/D)^{7/12}}{(4\pi\epsilon)^{5/12}} \qquad A_2 = \tfrac{2}{3}(4\pi\epsilon)^{1/2}(J/D)^{1/2} \qquad A_3 = \frac{1}{32\pi^2(J/D)\epsilon} \tag{8}$$

$$A_4 = 0.3787(J/D)^{19/12}\frac{(4\pi\epsilon)^{7/12}}{(9/D)}(d+1)^2 \qquad A_5 = \frac{(2d+1)(2d+2)}{32\pi^2(J/D^2)\epsilon} \tag{9}$$

for $d = 2$:

$$\begin{Bmatrix}\langle a\rangle\\ \langle b\rangle\end{Bmatrix} = (J/D)|x|\begin{Bmatrix}\theta(-x)\\ \theta(x)\end{Bmatrix} + B_1(\ln|x|)^{\frac{5}{12}}|x|^{-\frac{1}{4}}\mathrm{e}^{-B_2(\ln|x|)^{-1/2}|x|^{3/2}} + B_3|x|^{-5}\ln|x| + \cdots \tag{10}$$

$$R = B_4(\ln|x|)^{-7/12}|x|^{3/4}\mathrm{e}^{-B_2(\ln|x|)^{-1/2}|x|^{3/2}} + B_5|x|^{-7}\ln|x| + \cdots \tag{11}$$

where

$$B_1 = 0.3787\frac{(J/D)^{7/12}}{(4\pi)^{5/12}} \qquad B_2 = \tfrac{2}{3}(4\pi(J/D))^{1/2} \qquad B_3 = \frac{(J/D)^{-1}}{32\pi^2} \tag{12}$$

$$B_4 = 0.3787(4\pi)^{7/12}D(J/D)^{19/12} \qquad B_5 = \frac{15(J/D)^{-1}}{16\pi^2/D} \tag{13}$$

and finally, for $d > 2$:

$$\begin{Bmatrix}\langle a\rangle\\ \langle b\rangle\end{Bmatrix} = (J/D)|x|\begin{Bmatrix}\theta(-x)\\ \theta(x)\end{Bmatrix} + C_1|x|^{-1/4}\mathrm{e}^{-C_2|x|^{3/2}} + C_3|x|^{-d-3} + \cdots \tag{14}$$

$$R = C_4|x|^{3/4}\mathrm{e}^{-C_2|x|^{3/2}} + C_5|x|^{-d-5} + \cdots \tag{15}$$

where

$$C_1 = 0.3787\frac{(J/D)^{7/12}}{(\lambda/D)^{5/12}} \qquad C_2 = \tfrac{2}{3}(\lambda J/D^2)^{1/2} \tag{16}$$

$$C_3 = (\lambda J/D^2)^{-1}2^{-1-d}\pi^{-(d+1)/2}(d-1)\Gamma\left(\frac{d-1}{2}\right) \qquad C_4 = 0.3787\lambda\frac{(J/D)^{19/12}}{(\lambda/D)^{5/12}} \tag{17}$$

$$C_5 = \lambda(\lambda/D)^{-2}(J/D)^{-1}2^{-1-d}\pi^{-(d+1)/2}\Gamma\left(\frac{d-1}{2}\right)(d-1)(d+3)(d+4)\,. \tag{18}$$

Although these results are for the case of equal diffusion constants, our calculations could be repeated for $D_A \neq D_B$. However, we do not expect that such a modification will make a qualitative difference, at least for the case where both diffusion constants remain non-zero. Evidence for this comes from a similar calculation by Lee and Cardy [20] for the same two-species reaction, but with homogeneous initial conditions. They found that unequal diffusion constants only led to modified amplitudes for the densities, whilst leaving the density decay exponent unchanged.

The layout of this paper is as follows. In section 2, the system is defined using a master equation, which is then mapped to a second quantized representation, and then to a field theory. In section 3, we present two related field theories and derive the form of their Green functions. The renormalization of the theory is also addressed. The calculations for the densities and reaction front are presented in section 4, for $d < d_c$, $d = d_c$, and $d > d_c$. The separate problem of the fluctuations in the position of the centre of the reaction front is presented in section 5. A discussion of these results and comparisons with the available data from simulations are given in section 6, where we also argue for the presence of multiscaling in the system.

2. The model

We consider a model where particles A and B are moving diffusively on a hypercubic lattice, with lattice constant l. There is some probability of mutual annihilation whenever an A and a B particle meet on a lattice site. In addition, particles of type A are added at a constant rate to lattice sites on the hypersurface $x = -L$, and particles of type B are similarly added to sites at $x = L$. In other words, opposing currents of A and B particles are maintained at opposite edges of the system. The two hypersurfaces $x = \pm L$ mark the boundaries of the system beyond which the particles are not permitted to move. The model is defined by a master equation for $P(\{n, m\}, t)$, the probability of particle configuration $\{n, m\}$ occurring at time t. Here $\{n, m\} = (n_1, n_2, \ldots, n_N, m_1, m_2, \ldots, m_N)$, where n_i is the occupation number of the A particles, and m_i the occupation number of the B particles, at the ith lattice site. The appropriate master equation is

$$\begin{aligned}\frac{\partial}{\partial t}P(\{n,m\},t) = {} & \frac{D}{l^2}\sum_{i,e}\{(n_e+1)P(\ldots n_i-1, n_e+1, \ldots, \{m\}, t) - n_i P(\{n,m\},t)\} \\ & + \frac{D}{l^2}\sum_{i,e}\{(m_e+1)P(\{n\}, \ldots m_i - 1, m_e+1, \ldots, t) - m_i P(\{n,m\},t)\} \\ & + \lambda\sum_i[(n_i+1)(m_i+1)P(\ldots n_i+1, m_i+1\ldots, t) - n_i m_i P(\ldots n_i, m_i \ldots, t)] \\ & + R\{P(\ldots, n_{-L}-1, \{m\}, t) - P(\ldots, n_{-L}, \{m\}, t)\} \\ & + R\{P(\{n\}, m_L - 1\ldots, t) - P(\{n\}, m_L \ldots, t)\} \end{aligned} \tag{19}$$

where i is summed over lattice sites, and e is summed over the nearest neighbours of i. The first, second, and third lines of the equation describe diffusion of the A and B particles, respectively (with equal diffusion constants D), whilst the fourth line describes their annihilation within the system (with rate constant λ). The final four terms are due to the addition of particles A and B at the edges of the system at a rate R, corresponding to the maintenance of steady-particle currents.

The master equation can be mapped to a second quantized form, following a standard procedure developed by Doi [21] and Peliti [22], and as described by Lee [19]. In brief, in terms of the creation/annihilation operators $a, a^\dagger, b$ and $b^\dagger$ which are introduced at each lattice site, the time evolution operator for the system is

$$\hat{H} = -\frac{D}{l^2}\sum_{i,e}\{a_i^\dagger(a_e - a_i) + b_i^\dagger(b_e - b_i)\} - \lambda\sum_i(1 - a_i^\dagger b_i^\dagger)a_i b_i - R\{a_{-L}^\dagger - 1 + b_L^\dagger - 1\}. \tag{20}$$

This can now be mapped onto a path integral, in which $a, \hat{a}, b$ and $\hat{b}$ are replaced by continuous c-number fields, with action (up to a constant)

$$\begin{aligned} S = \sum_i\Bigg(\int_{-\infty}^{t} \mathrm{d}t\Bigg\{ & \hat{a}_i\dot{a}_i + \hat{b}_i\dot{b}_i - \frac{D}{l^2}\Big[\hat{a}_i\sum_e(a_e - a_i) + \hat{b}_i\sum_e(b_e - b_i)\Big] \\ & -\lambda(1 - \hat{a}_i\hat{b}_i)a_i b_i\Bigg\} - a_i(t) - b_i(t)\Bigg) \end{aligned} \tag{21}$$

where $a_i(t)$ and $b_i(t)$ are due to the projection state (see [19]), provided that

$$R = \frac{J}{l} = \frac{D}{l^2}(a_0 - a_{-L}) \qquad 0 = \frac{D}{l^2}(b_0 - b_{-L}) \tag{22}$$

at $-L$, and

$$R = \frac{J}{l} = \frac{D}{l^2}(b_0 - b_L) \qquad 0 = \frac{D}{l^2}(a_0 - a_L) \tag{23}$$

at $+L$. Here the sites $-L$, L are at the edges of the system, with site o being immediately outside L or $-L$. Taking the continuum limit of this action, we arrive at

$$S[\hat{a}, a, \hat{b}, b, t] = \int \left(\mathrm{d}x\, \mathrm{d}^{d-1}y \int_{-\infty}^{t} \mathrm{d}t \left\{ \hat{a}(\partial_t - D\nabla^2)a + \hat{b}(\partial_t - D\nabla^2)b \right.\right.$$
$$\left.\left. -\lambda_0(1 - \hat{a}\hat{b})ab \right\} - a(t) - b(t) \right). \tag{24}$$

subject to the conditions

$$-J = -D\partial_x b \qquad 0 = -D\partial_x a \tag{25}$$

at $+L$, and

$$J = -D\partial_x a \qquad 0 = -D\partial_x b \tag{26}$$

at $-L$. Here y are the coordinates for directions perpendicular to the applied currents. These conditions may be made explicit in the action by including a pair of delta functions:

$$S = \int \left(\mathrm{d}x\, \mathrm{d}^{d-1}y \int_{-\infty}^{t} \mathrm{d}t \left\{ \hat{a}(\partial_t - D\nabla^2)a + \hat{b}(\partial_t - D\nabla^2)b \right.\right.$$
$$\left.\left. -\lambda_0(1 - \hat{a}\hat{b})ab - \hat{a}J\delta(x + L) - \hat{b}J\delta(x - L) \right\} - a(t) - b(t) \right). \tag{27}$$

If we make the substitutions $\hat{a} = 1 + \bar{a}$ and $\hat{b} = 1 + \bar{b}$, then the action becomes (up to a constant)

$$S = \int \mathrm{d}x\, \mathrm{d}^{d-1}y\, \mathrm{d}t \left[\bar{a}(\partial_t - D\nabla^2)a + \bar{b}(\partial_t - D\nabla^2)b + \lambda_0 \bar{a}ab + \lambda_0 \bar{b}ab \right.$$
$$\left. +\lambda_0 \bar{a}\bar{b}ab - \bar{a}J\delta(x + L) - \bar{b}J\delta(x - L) \right]. \tag{28}$$

If we integrate over the $\bar{a}$ and $\bar{b}$ fields, and neglect the $\bar{a}\bar{b}ab$ term, we obtain the classical (mean-field) equations

$$(\partial_t - D\nabla^2)a + \lambda_0 ab - J\delta(x + L) = 0 \tag{29}$$
$$(\partial_t - D\nabla^2)b + \lambda_0 ab - J\delta(x - L) = 0. \tag{30}$$

On the further conditions that no particle annihilation occurs at the edges of the system, and that $\nabla a = 0$ and $\nabla b = 0$ outside, integrating the first equation from $-L - \epsilon$ to $-L + \epsilon$ and the second from $L - \epsilon$ to $L + \epsilon$ in the limit $\epsilon \to 0$ gives the required boundary conditions.

As the diffusion constant exhibits no singular behaviour in the renormalization of the theory, it is convenient to absorb it into a rescaling of time, as in [19]. Defining $\bar{t} = Dt$, $\bar{\lambda} = \lambda_0 D^{-1}$, and $\bar{J} = JD^{-1}$, and introducing the fields $\phi = \frac{1}{2}(a + b)$ and $\psi = \frac{1}{2}(a - b)$, we have

$$S = \int \mathrm{d}x\, \mathrm{d}^{d-1}y\, \mathrm{d}\bar{t} \left[2\bar{\phi}(\partial_{\bar{t}} - \nabla^2)\phi + 2\bar{\psi}(\partial_{\bar{t}} - \nabla^2)\psi + 2\bar{\lambda}\bar{\phi}(\phi^2 - \psi^2) \right.$$
$$+\bar{\lambda}(\bar{\phi}^2 - \bar{\psi}^2)(\phi^2 - \psi^2) - \bar{J}\bar{\phi}[\delta(x + L) + \delta(x - L)]$$
$$\left. -\bar{J}\bar{\psi}[\delta(x + L) - \delta(x - L)] \right]. \tag{31}$$

Consequently, the new classical equations of the steady state are

$$\partial_x^2 \psi_c + \tfrac{1}{2}\bar{J}[\delta(x + L) - \delta(x - L)] = 0 \tag{32}$$
$$\partial_x^2 \phi_c - \bar{\lambda}(\phi_c^2 - \psi_c^2) + \tfrac{1}{2}\bar{J}[\delta(x + L) + \delta(x - L)] = 0. \tag{33}$$

The appropriate solution for ψ_c is just $-(\bar{J}/2)x$ (for $|x| \leqslant L$), whilst substituting $\phi_c = (\bar{J}/2)|x| + u$ into the second equation gives asymptotically the Airy equation for u, as noted in [9]. Asymptotically one finds

$$\phi_c = \frac{J}{2D}|x| + 0.3787\left(\frac{J^2}{D\lambda}\right)^{1/3}\left(\frac{\lambda J}{D^2}\right)^{-1/12}|x|^{-1/4}\mathrm{e}^{-(2/3)(\lambda J D^{-2})^{1/2}|x|^{3/2}} + \cdots \tag{34}$$

where the constant was determined numerically.

So far the quartic term in the action has been neglected, with the result that the simple mean-field results have been recovered. However, we can take into account the non-classical term by including Gaussian noise in the equations for ϕ and ψ, leading to equations which are exact. This modification can be derived by replacing the quartic piece in the action by a noise variable, integrating over the noise distribution, and demonstrating that this recovers the original term. Observing that

$$\int_{-\infty}^{\infty} \mathrm{d}\eta_\phi \, \mathrm{e}^{\bar{\phi}\eta_\phi}\mathrm{e}^{-\eta_\phi^2/[4\bar{\lambda}(\phi^2-\psi^2)]} \sim \mathrm{e}^{\bar{\lambda}\bar{\phi}^2(\phi^2-\psi^2)} \tag{35}$$

and

$$\int_{-\infty}^{\infty} \mathrm{d}\eta_\psi \, \mathrm{e}^{\bar{\psi}\eta_\psi}\mathrm{e}^{-\eta_\psi^2/[4\bar{\lambda}(\phi^2-\psi^2)]} \sim \mathrm{e}^{-\bar{\lambda}\bar{\psi}^2(\phi^2-\psi^2)} \tag{36}$$

where η_ϕ and η_ψ are complex Gaussian noise variables with an appropriate phase, we see that the steady-state equations may be written as

$$\partial_x^2\psi + \tfrac{1}{2}\bar{J}[\delta(x+L) - \delta(x-L)] + \eta_\psi = 0 \tag{37}$$

$$\partial_x^2\phi - \bar{\lambda}(\phi^2 - \psi^2) + \tfrac{1}{2}\bar{J}[\delta(x+L) + \delta(x-L)] + \eta_\phi = 0\,. \tag{38}$$

Clearly we have lost the simple interpretation of the a and b fields as being the local densities of A and B particles, as now each of the above equations includes a (generally) complex noise term. Nevertheless, we can still interpret $\langle\psi\rangle$ and $\langle\phi\rangle$ as being averaged densities, which also satisfy

$$\partial_x^2\langle\psi\rangle + \tfrac{1}{2}\bar{J}[\delta(x+L) - \delta(x-L)] = 0 \tag{39}$$

$$\partial_x^2\langle\phi\rangle - \bar{\lambda}\langle\phi^2 - \psi^2\rangle + \tfrac{1}{2}\bar{J}[\delta(x+L) + \delta(x-L)] = 0\,. \tag{40}$$

The second equation will be used later on to relate a perturbation expansion for $\langle\phi\rangle$ to one for $\langle\phi^2 - \psi^2\rangle$.

Finally, we give the natural canonical dimensions for the various quantities appearing in the action, noting that the coupling becomes dimensionless at the postulated value of the critical dimension [15]:

$$[\bar{t}] = k^{-2} \qquad [a, b] = k^d \qquad [\bar{a}, \bar{b}] = k^0 \qquad [\bar{\lambda}] = k^{2-d} \qquad [\bar{J}] = k^{d+1}\,. \tag{41}$$

3. Field-theory formulations

In what follows it will be convenient to develop two parallel field theories—one given by the action already described in (31), and another to be described below, formed by writing $\phi = \phi_c + \phi_1$ and $\psi = \psi_c + \psi_1$. In particular, whilst the second theory is more useful for calculations, the cancellation of divergences after renormalization, and the identification of leading terms in an expansion in powers of the coupling constant, are easier to see in the first theory.

3.1. Propagators and vertices

The propagators for the first of the two theories described above (which we shall call field theory I) are (from (31))

$$G_{\phi\bar{\phi}}(k,\bar{t}) = G_{\psi\bar{\psi}}(k,\bar{t}) = \tfrac{1}{2}\mathrm{e}^{-k^2\bar{t}} \tag{42}$$

in $(k,\bar{t})$-space. In (k,s)-space, where a Laplace transform of time has been performed, we have

$$G_{\phi\bar{\phi}}(k,s) = G_{\psi\bar{\psi}}(k,s) = \frac{1}{2(k^2+s)}. \tag{43}$$

The vertices are shown in figure 1, where the ϕ propagators are represented by full lines, and ψ propagators by broken lines.

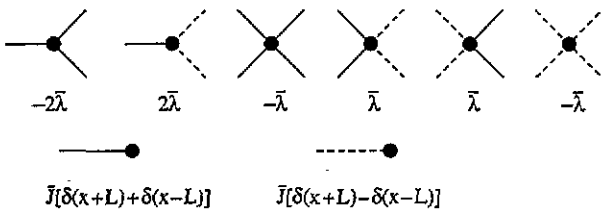

Figure 1. Vertices for field theory I.

For field theory II, we split the ϕ and ψ fields into their classical and non-classical components, which leads to a modified action

$$S = \int \mathrm{d}x\,\mathrm{d}^{d-1}y\,\mathrm{d}\bar{t}\big\{2\bar{\phi}(\partial_{\bar{t}} - \nabla^2 + 2\bar{\lambda}\phi_c)\phi_1 + 2\bar{\psi}(\partial_{\bar{t}} - \nabla^2)\psi_1$$
$$+2\bar{\lambda}\bar{\phi}(\phi_1^2 - \psi_1^2 - 2\psi_c\psi_1) + \bar{\lambda}(\bar{\phi}^2 - \bar{\psi}^2)(\phi_c^2 + 2\phi_c\phi_1 + \phi_1^2 - \psi_c^2 - 2\psi_c\psi_1 - \psi_1^2)\big\} \tag{44}$$

where the classical equations have been used to simplify its form somewhat. We can now substitute for the exact value of $\psi_c = -(\bar{J}/2)x$ and for the functional form of the ϕ_c field (from equation (33))

$$\phi_c = (\bar{J}^2/\bar{\lambda})^{1/3} f[(\bar{\lambda}\bar{J})^{1/3}x]. \tag{45}$$

If we also make the rescaling in the action of

$$\tilde{x} = (\bar{\lambda}\bar{J})^{1/3}x \qquad \tilde{y} = (\bar{\lambda}\bar{J})^{1/3}y \qquad \tilde{t} = (\bar{\lambda}\bar{J})^{2/3}\bar{t} \tag{46}$$

then it is transformed to

$$S = \int \mathrm{d}\tilde{x}\,\mathrm{d}^{d-1}\tilde{y}\,\mathrm{d}\tilde{t}(\bar{\lambda}\bar{J})^{-\frac{d}{3}}\big[2\bar{\phi}(\partial_{\tilde{t}} - \tilde{\nabla}^2 + 2f(\tilde{x}))\phi_1 + 2\bar{\psi}(\partial_{\tilde{t}} - \tilde{\nabla}^2)\psi_1$$
$$+2(\bar{\lambda}/\bar{J}^2)^{1/3}\bar{\phi}(\phi_1^2 - \psi_1^2) + 2\bar{\phi}\tilde{x}\psi_1$$
$$+(\bar{\phi}^2 - \bar{\psi}^2)\big((\bar{J}^2/\bar{\lambda})^{\frac{1}{3}}h(\tilde{x}) + 2f(\tilde{x})\phi_1 + \tilde{x}\psi_1 + (\bar{\lambda}/\bar{J}^2)^{\frac{1}{3}}(\phi_1^2 - \psi_1^2)\big)\big] \tag{47}$$

where

$$h(\tilde{x}) = [f(\tilde{x})]^2 - \tfrac{1}{4}\tilde{x}^2 \tag{48}$$

which is essentially just the classical profile of the reaction front. The form of the propagators is now

$$G_{\phi_1\bar{\phi}} = \tfrac{1}{2}(\bar{\lambda}\bar{J})^{d/3}G(\tilde{x},\tilde{x}',\tilde{y},\tilde{y}',\tilde{t}) \tag{49}$$

where

$$[\partial_{\tilde{t}} - \tilde{\nabla}^2 + 2f(\tilde{x})]G(\tilde{x},\tilde{x}',\tilde{y},\tilde{y}',\tilde{t}) = \delta(\tilde{x}-\tilde{x}')\delta(\tilde{y}-\tilde{y}')\delta(\tilde{t}-\tilde{t}') \tag{50}$$

and

$$G_{\psi_1\bar{\psi}}(\tilde{k},\tilde{s}) = \tfrac{1}{2}(\bar{\lambda}\bar{J})^{d/3}\frac{1}{\tilde{k}^2+\tilde{s}} \tag{51}$$

in $(\tilde{k},\tilde{s})$-space, or

$$G_{\psi_1\bar{\psi}}(\tilde{x}-\tilde{x}',\tilde{k}_\perp,\tilde{s}) = (\bar{\lambda}\bar{J})^{d/3}\frac{\mathrm{e}^{-(\tilde{k}_\perp^2+\tilde{s})^{1/2}|\tilde{x}-\tilde{x}'|}}{4(\tilde{k}_\perp^2+\tilde{s})^{1/2}} \tag{52}$$

in $(\tilde{x},\tilde{k}_\perp,\tilde{s})$-space, where the perpendicular directions are defined to be those perpendicular to the applied currents. Unfortunately, the equation for G (50) is too hard to solve exactly, as we do not have an analytic form for ϕ_c. Consequently, we must rely on the approximation $f(\tilde{x}) \sim \frac{1}{2}|\tilde{x}|$, valid at large $|\tilde{x}|$, in order to make the equation tractable. If we also Laplace transform time, and Fourier transform to momentum space for spatial dimensions perpendicular to the applied currents, then we obtain

$$\left(\tilde{s}+\tilde{k}_\perp^2-\partial_{\tilde{x}}^2+|\tilde{x}|\right)G(\tilde{x},\tilde{x}',\tilde{k}_\perp,\tilde{s}) = \delta(\tilde{x}-\tilde{x}')\,. \tag{53}$$

In appendix A, we show that for $\tilde{x} \approx \tilde{x}' \gg 0$, this gives

$$G_{\phi_1\bar{\phi}}(\tilde{x},\tilde{x}',\tilde{k}_\perp,\tilde{s}) = \tfrac{1}{4}(\bar{\lambda}\bar{J})^{d/3}(\tilde{x}+\tilde{k}_\perp^2+\tilde{s})^{-1/2}\mathrm{e}^{-(\tilde{x}+\tilde{k}_\perp^2+\tilde{s})^{1/2}|\tilde{x}-\tilde{x}'|}\,. \tag{54}$$

The important point to notice here is that for $\tilde{x}$ sufficiently close to $\tilde{x}'$, the Green function only decays as a power law.

Finally, we note that each occurrence of a propagator is associated with a factor of $(\bar{\lambda}\bar{J})^{d/3}$. If we also extract a factor of $(\bar{\lambda}\bar{J})^{-(d+2)/3}$ from each vertex, then we can use the vertices shown in figure 2, provided we multiply any given diagram by a factor of

$$(\bar{\lambda}\bar{J})^{\frac{1}{3}pd-\frac{v}{3}(d+2)} \tag{55}$$

where p is the number of propagators and v is the number of vertices. Again, in figure 2, ϕ propagators are full lines and ψ propagators are broken lines. Note the simple form of the vertices (h)–(m).

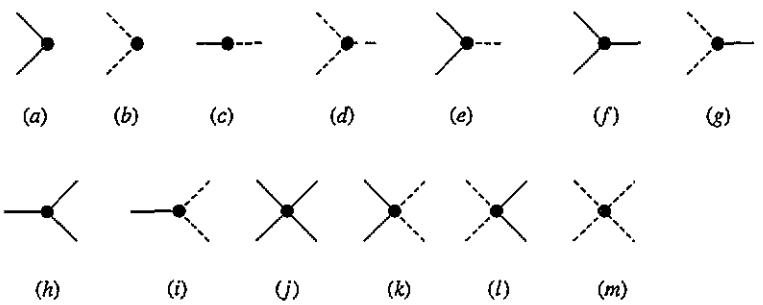

Figure 2. Vertices for field theory II. The couplings associated with each of the above diagrams are: (a) $-\bar{\lambda}^{1/3}\bar{J}^{4/3}h(\tilde{x})$, (b) $\bar{\lambda}^{1/3}\bar{J}^{4/3}h(\tilde{x})$, (c) $-2(\bar{\lambda}\bar{J})^{2/3}\tilde{x}$, (d) $(\bar{\lambda}\bar{J})^{2/3}\tilde{x}$, (e) $-(\bar{\lambda}\bar{J})^{2/3}\tilde{x}$, (f) $-2(\bar{\lambda}\bar{J})^{2/3}f(\tilde{x})$, (g) $2(\bar{\lambda}\bar{J})^{2/3}f(\tilde{x})$, (h) $-2\bar{\lambda}$, (i) $2\bar{\lambda}$, (j) $-\bar{\lambda}$, (k) $\bar{\lambda}$, (l) $\bar{\lambda}$ and (m) $-\bar{\lambda}$.

3.2. Renormalization

The renormalization of the theory proceeds in a similar vein to that described in [19]—our field theory differs only in the nature of the boundary conditions. Again the only renormalization required is coupling constant renormalization, as the set of vertices for field theory I allows no diagrams which dress the propagator. Hence we have no field renormalization and the bare propagators are the full propagators for the theory.

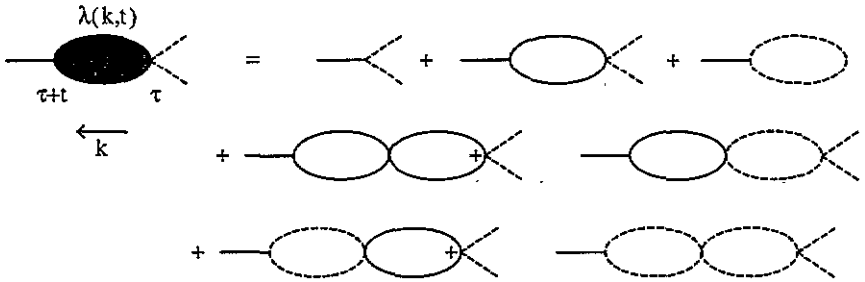

Figure 3. The sum of diagrams contributing to the primitively divergent vertex function $\lambda(k, t)$.

3.2.1. Renormalization of the coupling. The temporally extended vertex function for $A + B \to \emptyset$ is given by the sum of diagrams shown in figure 3. This sum may be calculated exactly, as was done in [20] (remembering extra factors of two resulting from the presence of two different types of propagator):

$$\bar{\lambda}(k, s) = \frac{\bar{\lambda}}{1 + \frac{1}{2}\bar{\lambda}B_2\Gamma(\epsilon/2)(s + \frac{1}{2}k^2)^{-\epsilon/2}} \tag{56}$$

where $B_2 = 2/(8\pi)^{d/2}$, and $\epsilon = 2 - d$. However, as we are now in the time-independent state, we take $s = 0$, leading to

$$\bar{\lambda}(k) = \frac{\bar{\lambda}}{1 + \frac{1}{2}\bar{\lambda}B_2\Gamma(\epsilon/2)2^{\epsilon/2}k^{-\epsilon}}\,. \tag{57}$$

The vertex function can now be used to define the renormalized coupling, with $k = \kappa$ as the normalization point (differing from [19]). So we have

$$g_R = \kappa^{-\epsilon}\bar{\lambda}(k)|_{k=\kappa} \qquad g_0 = \kappa^{-\epsilon}\bar{\lambda} \tag{58}$$

for the dimensionless renormalized and bare couplings, respectively. The β function is defined by

$$\beta(g_R) \equiv \kappa\frac{\partial}{\partial\kappa}g_R = -\epsilon g_R + \tfrac{1}{2}\epsilon g_R^2 B_2\Gamma(\epsilon/2)2^{\epsilon/2} \tag{59}$$

and we have a fixed point $\beta(g_R^*) = 0$ when

$$g_R^* = \{2^{-d/2}B_2\Gamma(\epsilon/2)\}^{-1}\,. \tag{60}$$

The fixed point is of order ϵ. Finally, the expansion of g_0 in powers g_R remains, as in [19]:

$$g_0 = g_R + \frac{g_R^2}{g_R^*} + \cdots. \tag{61}$$

3.2.2. Callan–Symanzik equation. We now write down the renormalization-group equation for $\langle\phi_1\rangle_R$ (the renormalized value of $\langle\phi_1\rangle$), expressing its lack of dependence on the normalization scale:

$$\left(\kappa\frac{\partial}{\partial\kappa} + \beta(g_R)\frac{\partial}{\partial g_R}\right)\langle\phi_1\rangle_R(x, g_R, \kappa, \bar{J}) = 0\,. \tag{62}$$

In addition, dimensional analysis implies

$$\left(\kappa\frac{\partial}{\partial\kappa} - x\frac{\partial}{\partial x} + (d+1)\bar{J}\frac{\partial}{\partial\bar{J}}\right)\langle\phi_1\rangle_R(x, g_R, \kappa, \bar{J}) = d\langle\phi_1\rangle_R(x, g_R, \kappa, \bar{J})\,. \tag{63}$$

Eliminating the terms involving κ, we have

$$\left(x\frac{\partial}{\partial x} - (d+1)\bar{J}\frac{\partial}{\partial \bar{J}} + \beta(g_R)\frac{\partial}{\partial g_R} + d\right)\langle\phi_1\rangle_R(x, g_R, \kappa, \bar{J}) = 0. \tag{64}$$

This can be solved by the method of characteristics, with solution

$$\langle\phi_1\rangle_R(x, g_R, \kappa, \bar{J}) = (\kappa x)^{-d}\langle\phi_1\rangle_R(\kappa^{-1}, \tilde{g}_R(\kappa^{-1}), \kappa, \tilde{\bar{J}}(\kappa^{-1})) \tag{65}$$

and associated characteristics

$$x\frac{\partial \tilde{g}_R}{\partial x} = \beta(\tilde{g}_R) \qquad \tilde{g}_R(x) = g_R \tag{66}$$

$$x\frac{\partial \tilde{\bar{J}}}{\partial x} = -(d+1)\tilde{\bar{J}} \qquad \tilde{\bar{J}}(x) = \bar{J}. \tag{67}$$

These equations have the exact solutions:

$$\tilde{\bar{J}}(x') = \left(\frac{x}{x'}\right)^{d+1}\bar{J} \tag{68}$$

$$\tilde{g}_R(x') = g_R^*\left(1 + \frac{g_R^* - g_R}{g_R\left(\frac{x}{x'}\right)^{\epsilon}}\right)^{-1} \tag{69}$$

where in the large-$|x|$ limit $\tilde{g}_R \to g_R^*$.

We can make use of the mechanics developed above by first calculating an expansion in powers of g_0, which can be converted into an expansion in powers of g_R via (61). Provided that the expansion is non-singular in ϵ, we can relate the g_R expansion to an ϵ expansion using (65), where for large $|x|$ we can take $\tilde{g}_R \to g_R^*$.

3.2.3. Tree diagrams. At this point we need to identify the leading terms in an expansion in powers of g_0—something which can be done in a very similar fashion to [19], using field theory I. For the calculation of $\langle\phi\rangle$, tree diagrams are of order $g_0^i\bar{J}^{1+i}$, for integer i. Diagrams with j loops will be of order $g_0^i\bar{J}^{1+i-j}$. As the addition of loops makes the power of g_0 higher relative to the power of $\bar{J}$, we see that the number of loops will give an indicator of the order of the diagram.

We are now in a position to develop two tree-level quantities—namely the classical density and the classical response function. Diagrammatically, we represent the classical densities by wavy lines and the classical response functions by thick lines. The tree-level density $\langle\phi\rangle$ is given by the sum of all tree diagrams which end with a $G_{\phi\bar{\phi}}$ propagator, as shown in figure 4(*b*). This is equivalent to the mean-field equation, as may be seen by acting on both sides of the graphical equation by the inverse Green function $2(\partial_\tau - \nabla^2)$. Similarly, acting on the much simpler tree-level diagram for $\langle\psi\rangle$ (figure 4(*a*)) with the inverse Green function gives its classical equation.

We now define the three response functions for the theory:

$$\begin{aligned}&\langle\psi(x, -k_\perp, -s)\bar{\psi}(x', k_\perp, s)\rangle^{(1)}\\ &\langle\phi(x, -k_\perp, -s)\bar{\phi}(x', k_\perp, s)\rangle^{(1)}\\ &\langle\phi(x, -k_\perp, -s)\bar{\psi}(x', k_\perp, s)\rangle^{(1)}\end{aligned} \tag{70}$$

where the superscript '1' indicates that they are defined in field theory I. Their diagrammatic sums are shown in figure 5. The first one: $\langle\psi(x, -k_\perp, -s)\bar{\psi}(x', k_\perp, s)\rangle^{(1)}$ is simply the propagator $G^{(2)}_{\psi_1\bar{\psi}}$, where the superscript '2' indicates that it belongs to

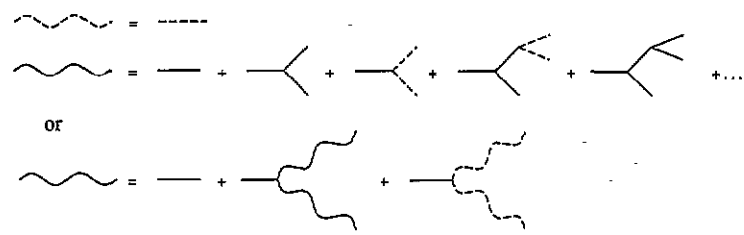

Figure 4. Tree level diagrams for (*a*) $\langle\psi\rangle$ and (*b*) $\langle\phi\rangle$.

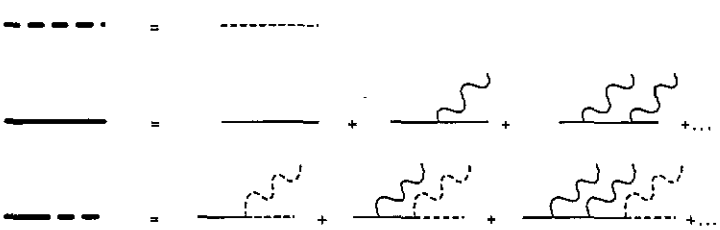

Figure 5. Response functions for field theory I: (*a*) $\langle\psi\bar{\psi}\rangle^{(1)}$, (*b*) $\langle\phi\bar{\phi}\rangle^{(1)}$ and (*c*) $\langle\phi\bar{\psi}\rangle^{(1)}$.

the second field theory. It is also easy to show that the second response function $\langle\phi(x, -k_\perp, -s)\bar{\phi}(x', k_\perp, s)\rangle^{(1)}$ is equivalent to the propagator $G^{(2)}_{\phi_1\bar{\phi}}$. To do this, we rearrange the unrescaled equation for $G^{(2)}_{\phi_1\bar{\phi}}$:

$$2(s + k_\perp^2 - \partial_x^2)G^{(2)}_{\phi_1\bar{\phi}}(x, x', k_\perp, s) = -4\bar{\lambda}\phi_c(x)G^{(2)}_{\phi_1\bar{\phi}}(x, x', k_\perp, s) + \delta(x - x')\,. \tag{71}$$

Including a delta-function integration in the first term on the right-hand side, and acting on both sides with the inverse Green function, we obtain

$$G^{(2)}_{\phi_1\bar{\phi}}(x, x', k_\perp, s) = G^{(1)}_{\phi\bar{\phi}} - 4\bar{\lambda}\int G^{(1)}_{\phi\bar{\phi}}(x, x_1, k_\perp, s)\phi_c(x_1)G^{(2)}_{\phi_1\bar{\phi}}(x_1, x', k_\perp, s)\,\mathrm{d}x_1 \tag{72}$$

where $G^{(1)}_{\phi\bar{\phi}}$ is the ϕ propagator for the first field theory. Iteration now generates the appropriate tree-level expansion for $\langle\phi(x, -k_\perp, -s)\bar{\phi}(x', k_\perp, s)\rangle^{(1)}$, and we have $G^{(2)}_{\phi_1\bar{\phi}} = \langle\phi\bar{\phi}\rangle^{(1)}$. The remaining response function $\langle\phi\bar{\psi}\rangle^{(1)}$ is, as would be expected, equivalent in the second field theory to the two-point vertex sandwiched between a ϕ propagator and a ψ propagator.

4. Density and reaction front calculations

We first note that we cannot draw diagrams which terminate with a ψ_1 propagator in field theory II. Consequently, we conclude that $\langle\psi_1\rangle = 0$, and hence that $\langle\psi\rangle = \psi_c$. This also follows from averaging equation (37). We now turn to the asymptotic evaluation of $\langle\phi\rangle$. Inserting the classical (tree-level) solution (34) into the Callan–Symanzik solution (65), and making the leading-order replacements $\bar{\lambda} \to g_R\kappa^\epsilon$, and for large $|x|$, $\bar{g}_R \to g_R^*$, we obtain

$$\langle\phi\rangle = \tfrac{1}{2}\bar{J}|x| + 0.3787\frac{\bar{J}^{7/12}}{g_R^{*\,5/12}}|x|^{(7-5d)/12}\mathrm{e}^{-(2/3)g_R^{*\,1/2}\bar{J}^{1/2}|x|^{(d+1)/2}} + \cdots\,. \tag{73}$$

If we use the explicit value of g_R^* from (60), then

$$\langle\phi\rangle = \tfrac{1}{2}\bar{J}|x| + 0.3787\frac{\bar{J}^{7/12}}{(4\pi\epsilon)^{5/12}}|x|^{(7-5d)/12}\mathrm{e}^{-(2/3)(4\pi\epsilon)^{1/2}\bar{J}^{1/2}|x|^{(d+1)/2}} + \cdots\,. \tag{74}$$

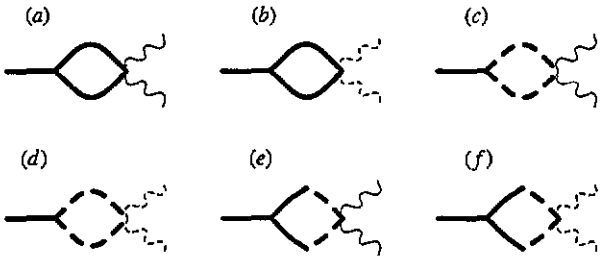

Figure 6. One-loop diagrams in field theory I.

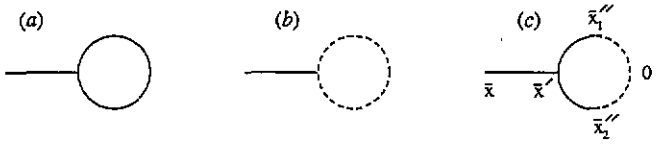

Figure 7. One-loop diagrams in field theory II.

So the tree-level expression consists of the expected linear term, which must be present if the boundary conditions are to be satisfied, together with a stretched exponential component.

4.1. One-loop contributions

According to our earlier arguments we expect the next order contributions to $\langle\phi\rangle$ (in field theory I) to contain a one-loop embedded somewhere in the tree diagram. The diagrams corresponding to this prescription are shown in figure 6. However, we have shown that we may translate these diagrams into field theory II by replacing response functions by propagators. This is convenient as we have analytic expressions for the Green functions in the second field theory (at least asymptotically), and so performing calculations becomes easier. The equivalent diagrams for field theory II are shown in figure 7. Notice that the density lines present in the diagrams for field theory I have been absorbed into the vertices for field theory II, where a factor of $\phi_c^2 - \psi_c^2$ is present at the source vertex.

We begin by calculating the third diagram of figure 7. At this level of approximation, we replace the source (the incoming classical density lines at the rightmost vertex in field theory I) by a delta function at the origin, with a weight equal to the area under the classical reaction front; in other words:

$$\phi_c^2 - \psi_c^2 \to \left(\int (\phi_c^2 - \psi_c^2) \mathrm{d}x' \right) \delta(x) . \tag{75}$$

This will be valid provided $\langle\phi\rangle$ decays much more slowly than the classical reaction front—an assumption that will be shown to be justified *a posteriori*. By integrating the classical equations, we also have the relation

$$\bar{\lambda} \int (\phi_c^2 - \psi_c^2) \, \mathrm{d}x' = \bar{\lambda}^{1/3} \bar{J}^{4/3} \int h[(\bar{\lambda}\bar{J})^{1/3} x'] \, \mathrm{d}x' = \bar{J} \tag{76}$$

which is simply saying that, classically, the number of particles entering the system is the same as the number being annihilated at the reaction front. This relationship is also true non-classically, if we average over the noise. After we have performed the rescaling

$\tilde{x}' = (\bar{\lambda}\bar{J})^{1/3}x'$, this becomes

$$\int h(\tilde{x}')\,\mathrm{d}\tilde{x}' = 1\,. \tag{77}$$

So the vertex factor at the source becomes

$$\bar{\lambda}^{1/3}\bar{J}^{4/3}h(\tilde{x}) \to \bar{\lambda}^{1/3}\bar{J}^{4/3}\left(\int h(\tilde{x}')\,\mathrm{d}\tilde{x}'\right)\delta(\tilde{x}) = \bar{\lambda}^{1/3}\bar{J}^{4/3}\delta(\tilde{x})\,. \tag{78}$$

The evaluation of the diagram is presented in appendix B, where it is shown that part of the result cancels off the (divergent) diagram shown in figure 7(*b*). The net result of these two diagrams is then

$$-(\bar{\lambda}\bar{J})^{-1}2^{-1-d}\pi^{-(d+1)/2}(1-d)\Gamma\left(\frac{d-1}{2}\right)x^{-d-3}\,. \tag{79}$$

We may now insert this into the Callan–Symanzik solution (65), and use the results for the running current/coupling (68)/(69), and for the coupling fixed point (60). This leads to the *one-loop density correction*

$$\frac{x^{-2d-1}}{32\pi^2\bar{J}\epsilon} \tag{80}$$

which justifies the use of the delta function approximation for the source. The one remaining diagram in figure 7 consists entirely of ϕ propagators, and so asymptotically we expect an exponential dependence which we neglect in comparison with the power law. So to this level of accuracy, we have

$$\langle\phi\rangle = \tfrac{1}{2}\bar{J}|x| + 0.3787\frac{\bar{J}^{7/12}}{(4\pi\epsilon)^{5/12}}|x|^{(7-5d)/12}\mathrm{e}^{-\frac{2}{3}(4\pi\epsilon)^{1/2}\bar{J}^{1/2}|x|^{(d+1)/2}} + \frac{|x|^{-2d-1}}{32\pi^2\bar{J}\epsilon} + \cdots. \tag{81}$$

Using the relation (40) it is also straightforward to calculate the form of the reaction front profile:

$$R = \lambda\langle\phi^2 - \psi^2\rangle = 0.3787\bar{J}^{19/12}\frac{(4\pi\epsilon)^{7/12}}{9/D}(d+1)^2|x|^{(7d-5)/12}\mathrm{e}^{-\frac{2}{3}(4\pi\epsilon)^{1/2}\bar{J}^{1/2}|x|^{(d+1)/2}} + \frac{(2d+1)(2d+2)|x|^{-2d-3}}{32\pi^2\epsilon\bar{J}/D} + \cdots \tag{82}$$

where only the leading terms generated by the differentiation of each of the component parts of (81) have been retained.

Finally, we consider the cancellation of divergences at one-loop which, as we mentioned earlier, can most easily be seen in the formalism of field theory I. We expect divergent contributions from the one-loop diagrams (*a*)–(*d*) in figure 6, in the limit where the position of the loop's left vertex tends towards that of the right vertex. In this limit, where no insertions are possible into the response functions, it is appropriate to replace the loop of the ϕ response functions with one of the ψ response functions. Evaluating this loop gives the result $1/2g_R^*$, and the diagrams become as shown in figure 8. However, if we consider the corrections to the tree level due to subleading terms in $g_0(g_R)$ (from equation (61)), we have the same diagrams but with opposite signs, which exactly cancel the one-loop divergences.

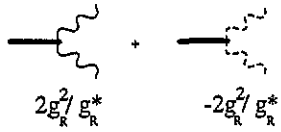

Figure 8. Divergences at one-loop. The factor underneath each diagram is associated with the vertex.

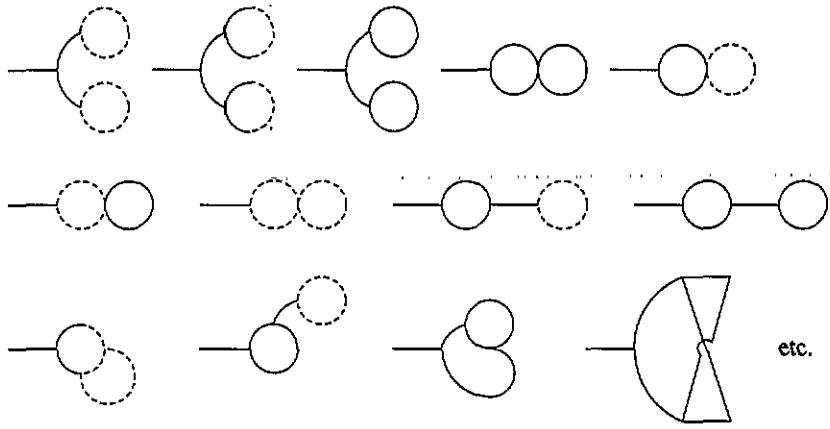

Figure 9. A sample of the two-loop diagrams for $\langle\phi_1\rangle$.

4.1.1. Two loops. Whilst we have not calculated in full the contributions to the density from the two-loop diagrams, a remark concerning their general nature, and of the nature of our perturbation expansion, is in order. A sample of these two-loop diagrams is shown in figure 9.

The easiest diagrams to evaluate are the first and second of those in figure 9, for which it is easy to check that they have the form

$$\sim \frac{|x|^{-4d-3}\bar{J}^{-3}}{\epsilon^2} \sim \epsilon^{-1/2}|x|^{-d}\left[\bar{J}|x|^{d+1}\epsilon^{1/2}\right]^{-3}. \tag{83}$$

Hence the perturbative expansion for the power-law contributions to $\langle\phi\rangle$ would appear to have the form:

$$\langle\phi\rangle \sim \epsilon^{-\frac{1}{2}}|x|^{-d}\left[\bar{J}|x|^{d+1}\epsilon^{1/2}\right] + \epsilon^{-\frac{1}{2}}|x|^{-d}\left[\bar{J}|x|^{d+1}\epsilon^{1/2}\right]^{-1} + \epsilon^{-\frac{1}{2}}|x|^{-d}\left[\bar{J}|x|^{d+1}\epsilon^{1/2}\right]^{-3} + \cdots. \tag{84}$$

Consequently, we see that the condition for our field theory to be valid is that the dimensionless parameter $\bar{J}|x|^{d+1}$ be $\gg 1$. It should also be noted that subleading power laws from the loop integrals will be smaller than their leading term by factors of $(\bar{J}|x|^{d+1})^{-1/3}$.

4.2. $d \geqslant 2$

At the upper critical dimension for the system, in this case $d = 2$, we expect logarithmic corrections to the $d > 2$ results, owing to the presence of the marginally irrelevant parameter $\bar{\lambda}$. The Callan–Symanzik solution (65) is still valid, although with a different coupling, which we calculate by taking $\epsilon \to 0$ in (59). This gives the running coupling

$$\tilde{g}_R(\kappa^{-1}) = \frac{g_R}{1 + \frac{g_R}{4\pi}\ln(\kappa x)}. \tag{85}$$

The behaviour of the running current is as previously calculated. Using the asymptotic form $\tilde{g}_R \sim 4\pi/\ln(\kappa x)$, we obtain

$$\langle\phi\rangle = \tfrac{1}{2}\bar{J}|x| + 0.3787\bar{J}^{7/12}\left(\frac{\ln|x|}{4\pi}\right)^{5/12}|x|^{-\frac{1}{4}}\mathrm{e}^{-\frac{2}{3}(4\pi\bar{J})^{1/2}(\ln|x|)^{-1/2}|x|^{3/2}} + \frac{|x|^{-5}\ln|x|}{32\pi^2\bar{J}} + \cdots \tag{86}$$

where higher-order corrections will be only $O[(\ln|x|)^{-1}]$ smaller, so the asymptotic regime will be accordingly hard to reach. Finally, for the reaction front, we have

$$R = 0.3787D\frac{(4\pi)^{7/12}\bar{J}^{19/12}}{(\ln|x|)^{7/12}}|x|^{3/4}\mathrm{e}^{-\frac{2}{3}(4\pi\bar{J})^{1/2}(\ln|x|)^{-1/2}|x|^{3/2}} + \frac{15D\bar{J}^{-1}|x|^{-7}\ln|x|}{16\pi^2} + \cdots . \tag{87}$$

For dimensions higher than the critical dimension, the expressions from the evaluation of the Feynman diagrams are used directly without being inserted into the Callan–Symanzik solution. This gives us the results, valid for $d > 2$, and in the regime $(J^2\lambda/D^3)|x|^{d+4} \gg 1$:

$$\langle\phi\rangle = \tfrac{1}{2}\bar{J}|x| + 0.3787\frac{\bar{J}^{7/12}}{\bar{\lambda}^{5/12}}|x|^{-1/4}\mathrm{e}^{-\frac{2}{3}(\bar{\lambda}\bar{J})^{1/2}|x|^{3/2}} - (\bar{\lambda}\bar{J})^{-1}2^{-1-d}\pi^{-(d+1)/2}(1-d)\Gamma\left(\frac{d-1}{2}\right)|x|^{-d-3} + \cdots \tag{88}$$

and

$$R = 0.3787\bar{J}^{19/12}\bar{\lambda}^{7/12}D|x|^{3/4}\mathrm{e}^{-\frac{2}{3}(\bar{\lambda}\bar{J})^{1/2}|x|^{3/2}} - D\bar{\lambda}^{-1}\bar{J}^{-1}2^{-1-d}\pi^{-(d+1)/2}\Gamma\left(\frac{d-1}{2}\right)(1-d)(d+3)(d+4)|x|^{-d-5} + \cdots . \tag{89}$$

5. Interface fluctuations

We now turn to the related problem of the nature of fluctuations in position of the reaction front. This is similar to the question of the fluctuations of an interface in the dynamical Ising model, as described by the time-dependent Landau–Ginzburg (TDLG) equation with noise (for example in model A, see [25]). This equation may be mapped to a path integral for the field Φ, with the introduction of response fields $\tilde{\Phi}$, using the Martin–Siggia–Rose formalism:

$$\int \mathcal{D}\Phi\,\mathcal{D}\tilde{\Phi}\mathrm{e}^{-\int \mathrm{d}x\,\mathrm{d}^{d-1}y\,\mathrm{d}t[\tilde{\Phi}\{\dot{\Phi}+\Gamma(\nabla^2\Phi+V'(\Phi))\}+\frac{1}{2}\Gamma\tilde{\Phi}^2]} \tag{90}$$

where the last term in the action results from averaging over the noise. Solving the TDLG equation in the absence of noise gives us the classical profile Φ_c, and on physical grounds we expect the full functional form of Φ to be $\Phi_c(x - f(y,t)) \approx \Phi_c(x) - f(y,t)\Phi_c'(x)$. The idea now is to substitute this into the action and to expand the response fields in terms of some complete set of eigenfunctions $\Psi_n(x)$:

$$\tilde{\Phi}(x,y,t) = \sum_n A_n\tilde{f}_n(y,t)\Psi_n(x) \tag{91}$$

where the $\{A_n\}$ are normalizing constants. This set is chosen such that when the x dependence is integrated out of the action, it leaves behind an unambiguous equation for $f(y,t)$, obtained by integrating over the new response fields $\tilde{f}(y,t)$ in the path integral. For the Ising case, $f(y,t)$ can be shown to satisfy a noisy diffusion equation, whose solution

implies that fluctuations delocalize the interface for $d \leqslant 3$. A similar result for reaction fronts would have dramatic consequences.

Returning to the reaction–diffusion system, we expect the functional forms for the fields in our geometry to be $\psi(x - f_1(y,t))$ and $\phi(x - f_2(y,t))$, by analogy with the Ising case. Considering first the situation where we neglect noise in the system, we expand the above functional forms, giving

$$\phi \approx \phi(x) - f_2(y,t)\phi'(x) \Rightarrow \phi = \tfrac{1}{2}\bar{J}|x| \mp \tfrac{1}{2}\bar{J}f_2 \qquad (x = \pm L) \tag{92}$$

$$\psi = \psi(x) - f_1(y,t)\psi'(x) \Rightarrow \psi = -\tfrac{1}{2}\bar{J}x + \tfrac{1}{2}\bar{J}f_1 . \tag{93}$$

Hence $a = \frac{1}{2}\bar{J}(f_1 - f_2)$ and $b = \bar{J}x - \frac{1}{2}\bar{J}(f_1 + f_2)$ at $x = L$, and $a = -\bar{J}x + \frac{1}{2}\bar{J}(f_1 + f_2)$ and $b = \frac{1}{2}\bar{J}(f_2 - f_1)$ at $x = -L$. In the absence of noise a and b represent the (positive) particle densities, so we must have $f_1 = f_2$.

However, if we include the noise term then this argument is invalid, and we proceed, as in the Ising case, by inserting the expanded functional forms for ϕ and ψ into the action for field theory I, giving

$$S = \int \mathrm{d}x\, \mathrm{d}^{d-1}y\, \mathrm{d}t[2\bar{\phi}\{\phi_c'[-\dot{f}_2 + \nabla_\perp^2 f_2] + 2\bar{\lambda}\psi_c\psi_c'(f_1 - f_2)\}$$
$$+2\bar{\psi}\{\psi_c'[-\dot{f}_1 + \nabla_\perp^2 f_1]\} + \bar{\lambda}(\bar{\phi}^2 - \bar{\psi}^2)(\phi_c^2 - \psi_c^2)] \tag{94}$$

where we have made the approximation $\phi \to \phi_c$, and then used the classical equations to simplify the expression. Here y are the coordinates for directions perpendicular to the applied currents. In our case it is now appropriate to Fourier expand the $\bar{\psi}$ and $\bar{\phi}$ fields, i.e.

$$\bar{\psi} = \sum_n \zeta_n(y,t)\theta_n(x) \qquad \bar{\phi} = \sum_n \xi_n(y,t)\theta_n(x) \tag{95}$$

where $\theta_n = \sin(n\pi x/L)$ for $n > 0$, $\theta_n = \frac{1}{2}$ for $n = 0$, and $\theta_n = \cos(n\pi x/L)$ for $n < 0$. Inserting this into the noise term and performing the x integration, we have

$$\int \bar{\psi}^2(\phi_c^2 - \psi_c^2)\mathrm{d}x = \sum_{n,m} \zeta_n\zeta_m \int_{-L}^{L} \theta_n\theta_m(\phi_c^2 - \psi_c^2)\mathrm{d}x = \sum_{n,m} \zeta_n X_{nm}\zeta_m \tag{96}$$

where X_{nm} is a symmetric matrix which we now diagonalize. Using $\hat{\zeta}_n = D_{nm}\zeta_m$, but such that $\hat{\zeta}_0 = \zeta_0$, we rewrite (96) as

$$\sum_{n,m} \hat{\zeta}_n \Lambda_{nm} \hat{\zeta}_m \tag{97}$$

where Λ is a diagonal, and $\mathbf{D}$ a diagonalizing, matrix. Bearing in mind the symmetries of the classical solutions, we can perform the x integration within the action to arrive at the path integral:

$$\int \mathcal{D}f_1\, \mathcal{D}f_2 \prod_n \mathcal{D}\hat{\zeta}_n\, \mathcal{D}\xi_n \exp\Big[-\int \mathrm{d}^{d-1}y\, \mathrm{d}t\Big\{2\sum_{n>0} \xi_n[A_n(-\dot{f}_2 + \nabla_\perp^2 f_2) + 2\bar{\lambda}B_n(f_1 - f_2)]$$
$$+\bar{\lambda}\sum_{n,m} \xi_n\xi_m X_{nm} + 2\hat{\zeta}_0 C_0[-\dot{f}_1 + \nabla_\perp^2 f_1] - \bar{\lambda}\sum_n \hat{\zeta}_n\Lambda_{nn}\hat{\zeta}_n\Big\}\Big] \tag{98}$$

with

$$A_n = \int_{-L}^{L} \theta_n\phi_c'\,\mathrm{d}x \qquad B_n = \int_{-L}^{L} \theta_n\psi_c\psi_c'\,\mathrm{d}x \qquad C_0 = \int_{-L}^{L} \theta_0\psi_c'\,\mathrm{d}x \sim \bar{J}L . \tag{99}$$

Integrating over $\hat{\xi}_0$ and f_1 gives the equation

$$-\dot{f}_1 + \nabla_\perp^2 f_1 + \eta = 0 \tag{100}$$

where η is a (possibly imaginary) noise variable, with a Gaussian distribution

$$P(\eta) \sim \mathrm{e}^{-(\eta^2 C_0^2/\bar{\lambda}|\Lambda_{00}|)}. \tag{101}$$

If we also diagonalize the noise term involving the ξ fields, then the relevant part of the action is transformed to

$$2\sum_{n>0} W_n \hat{\xi}_n [A_n(\dot{g} - \nabla_\perp^2 g - \eta) - 2\bar{\lambda} B_n g] + \bar{\lambda} \sum_n \hat{\xi}_n \Lambda_{nn} \hat{\xi}_n \tag{102}$$

where $g = f_1 - f_2$, and the equation for f_1 (100) has been added into the action. The $\{W_n\}$ are coefficients generated by writing ξ_n in terms of $\{\hat{\xi}_m\}$. Finally, performing the integrations over $\hat{\xi}_n$ and g, we find equations for g which can only be mutually consistent for different n if $g = 0$, or in other words, if $f_1 = f_2 = f$. From equation (96) we see that $\Lambda_{00} \sim \bar{J}\bar{\lambda}^{-1}$, and so

$$-\dot{f} + \nabla_\perp^2 f + \eta = 0 \tag{103}$$

where η is a Gaussian noise variable with probability distribution:

$$P(\eta) \sim \mathrm{e}^{-(\text{constant})L^2 \bar{J}\eta^2}. \tag{104}$$

We now proceed to calculate the mean-square fluctuation $\langle f^2 \rangle - \langle f \rangle^2$. This can be done in a straightforward manner, solving the noisy diffusion equation satisfied by f using a Green function method. The results are

$$\langle f(y,t)^2 \rangle - \langle f(y,t) \rangle^2 \sim \begin{cases} \dfrac{\Lambda^{d-3}\bar{J}^{-1}}{L_\parallel^2} & \text{for} \quad d \geqslant 4 \\ \dfrac{\ln(L_\perp \Lambda)\bar{J}^{-1}}{L_\parallel^2} & \text{for} \quad d = 3 \\ \dfrac{L_\perp \bar{J}^{-1}}{L_\parallel^2} & \text{for} \quad d = 2 \end{cases} \tag{105}$$

where the system has physical dimensions $L_\parallel \times L_\perp^{d-1}$, and Λ is now the large k momentum cut-off. So we expect that interface fluctuations will be unimportant if

$$\langle f^2 \rangle - \langle f \rangle^2 \sim \begin{cases} \dfrac{\Lambda^{d-3}}{L_\parallel^2 J D^{-1}} \ll L_\parallel^2 \quad \Rightarrow \quad \dfrac{L_\parallel^2 (JD^{-1})^{1/2}}{\Lambda^{(d-3)/2}} \gg 1 & \text{for} \quad d \geqslant 4 \\ \dfrac{\ln(L_\perp \Lambda)}{L_\parallel^2 J D^{-1}} \ll L_\parallel^2 \quad \Rightarrow \quad \dfrac{L_\parallel^2 (JD^{-1})^{1/2}}{(\ln(L_\perp \Lambda))^{1/2}} \gg 1 & \text{for} \quad d = 3 \\ \dfrac{L_\perp}{L_\parallel^2 J D^{-1}} \ll L_\parallel^2 \quad \Rightarrow \quad \dfrac{L_\parallel^2 (JD^{-1})^{1/2}}{L_\perp^{1/2}} \gg 1 & \text{for} \quad d = 2. \end{cases} \tag{106}$$

These results can now be applied to the problem of the late-time behaviour of an initially homogeneous distribution of A and B particles [26–29], where it has been shown that the reactants segregate asymptotically [26, 29]. Here we assume that we can access the quasistatic time-dependent regime by simply replacing our currents J by their time-dependent analogues (this point is discussed further in the next section). In [29] it is demonstrated that these time-dependent inward currents (towards the domain interfaces) scale as $J \sim t^{-(d+2)/4}$, where the domains have a characteristic length scale which grows

in time as $t^{1/2}$. So on the basis of our assumption we can insert the appropriate time dependencies into (106), from where it is easily seen that fluctuations are unimportant for large enough t, in dimensions where segregation occurs ($d < 4$).

6. Discussion

The main results of our earlier calculations are expansions for the asymptotic behaviour of the density and reaction front profiles for dimensions above, below, and equal to the critical dimension. We now compare our analytic results with the available data from recent numerical simulations [6, 10, 15, 17, 18]. Note that in all of these papers except [15], the initial conditions are those of complete particle segregation—so the particle currents at later times are time dependent. The remaining reference [15] contains the results of simulations in the steady state. As we mentioned in the introduction, the calculations of this paper can, in principle, be redone for the time-dependent case. However, simple one-loop considerations for $\langle\psi^2\rangle$ indicate that the dominant contributions to the integrals originate from large times. At these times the reaction front is formed quasistatically, and so we expect to be able to relate to the steady-state case by making the correspondence $J \sim t^{-1/2}$ [18, 29] (but see below for occasions where this breaks down). Data for $d = 2$ in the time-dependent situation is presented in [6, 10], although in [6] there is insufficient information to extract the asymptotic behaviour of the reaction front. Further simulations for $d = 2$ and also for $d = 1, 3$ are given in [15], where evidence for (5)—their proposed scaling form of R is given. The reaction front profile is seen to exhibit good scaling collapse close to its centre for $d = 1, 2, 3$ but again no information is available for the asymptotics addressed in this paper.

Turning now to the 1D case, the simulations in [17, 18] were performed using an infinite reaction rate constant, i.e. if two particles of different species either crossed or occupied the same lattice site, they immediately annihilated. With initial conditions of complete particle segregation, this resulted in total separation of the two species at all later times. Consequently, the reaction front profile was determined by the fluctuations in position of a delta-function like reaction front. Our results are for finite reaction rates, and are dominated by density fluctuations which propagate out from the reaction front centre to positions far away, a process which cannot occur in the 1D simulations mentioned above. We believe this to be the reason for the discrepancy between our analytic calculations and the numerical results. For example, the 1D simulations of Cornell produce evidence for a Gaussian reaction front profile, most notably in figure 8 of [18], in which $\log R$ is plotted against $(x/X^{(2)})^2$, where $X^{(2)}$ is the width of the reaction *product* profile $C = \int R(x,t)dt$, as measured by its second spatial moment. The resulting straight line indicates that the Gaussian profile is maintained well into the asymptotic region (i.e. at least as far as $(x/X^{(2)})^2 \approx 30$)—in exactly the region where, in our model, we would expect our asymptotic expansion to begin to apply.

In addition, controversy still exists over the spatial moments of the reaction front profile—Araujo *et al* [17] and Cornell [18] disagree over the presence of multiscaling. In fact, our calculations suggest that multiscaling does indeed occur for high enough moments in the time-dependent version of our model, starting from completely segregated initial conditions. For the steady-state situation, the existence of the asymptotic power laws found

above implies that the moments

$$x^{(q)} = \left(\frac{\int_{-\infty}^{\infty} |x|^q R(x)\,\mathrm{d}x}{\int_{-\infty}^{\infty} R(x)\,\mathrm{d}x} \right)^{1/q} \tag{107}$$

do not exist for $q \geqslant \mu + 1$. However, in the time-dependent case, these moments must exist due to the presence of a diffusive cut-off at $x_D \sim t^{1/2}$ [30]. Therefore, for the calculation of the spatial moments $x^{(q)}$ (for large enough q), we cannot relate the steady-state case to the time-dependent case by simply applying the scaling substitution $J \sim t^{-1/2}$. We can make these remarks more quantitative by performing the calculation of the spatial moments in the time-dependent situation. Separate arguments must be applied for $d < 2$, when our RG arguments imply that the steady-state profile has a scaling form (82); and for $d > 2$, when (89) shows that the fluctuation-induced power-law tails do not scale. For $d < 2$, we have:

$$x^{(q)}(t) \sim \left(\frac{\int_{-\infty}^{\infty} |x|^q t^{-\beta} S\left(\frac{x}{t^{\alpha}}\right) F\left(\frac{x}{t^{1/2}}\right) \mathrm{d}x}{\int_{-\infty}^{\infty} t^{-\beta} S\left(\frac{x}{t^{\alpha}}\right) F\left(\frac{x}{t^{1/2}}\right) \mathrm{d}x} \right)^{1/q} \tag{108}$$

where α and β are defined in the usual way [1, 29]. Here $F(y)$ is a function which provides a cut-off at $y \sim \mathrm{O}(1)$, but whose inclusion does not affect the calculation of moments which are finite even in the absence of a cut-off. For $q < \mu + 1$, where the qth moment of S is finite (even without a cut-off), we can therefore neglect the effects of F. However, for $q > \mu + 1$, the qth moment is infinite without the cut-off, so the integral will now be *dominated by the region $(x/t^{1/2}) \sim \mathrm{O}(1)$, where the asymptotic result $S \sim (x/t^{\alpha})^{-\mu-2}$* may be used. These considerations lead to the result $x^{(q)}(t) \sim t^{\alpha_q}$, where (neglecting any logarithmic corrections for $q = \mu + 1$):

$$\alpha_q = \begin{cases} \alpha & \text{for} \quad q < \mu + 1 \\ \dfrac{1}{2} + \dfrac{(\mu+1)\left(\alpha - \frac{1}{2}\right)}{q} & \text{for} \quad q > \mu + 1\,. \end{cases} \tag{109}$$

Hence we have a cusp at $q = \mu + 1$, above which α_q tends towards $\frac{1}{2}$ for large q. Note that this value of $\frac{1}{2}$ is specific to a diffusive cut-off of the form $F(x/t^{1/2})$. For $d = 2$ we also expect logarithmic corrections to the above power laws.

For $d > 2$, we must carry out a slightly different calculation, as although the classical (tree-level) reaction front obeys scaling, equation (89) reveals that the one-loop power law correction does not. However, for moments which exist without a cut-off, it turns out that *the classical terms still give the dominant contribution in the scaling limit.* For these terms we have, in the steady-state case,

$$\int_{-\infty}^{\infty} |x|^q R_c(x, \lambda, J)\,\mathrm{d}x \sim \lambda^{1/3} J^{4/3} \int_{-\infty}^{\infty} |x|^q S_c[(\lambda J)^{1/3} x]\,\mathrm{d}x \sim \lambda^{-q/3} J^{1-q/3}\,. \tag{110}$$

However, for the non-scaling power law we must consider

$$(\lambda J)^{-1} \int_{(\lambda J^2)^{-1/(d+4)}}^{\infty} \frac{x^q\,\mathrm{d}x}{x^{d+5}} \sim \lambda^{-q/(d+4)} J^{1-2q/(d+4)} \tag{111}$$

where we have imposed a lower cut-off in the integral derived from the expansion parameter of the $d > 2$ asymptotic series (89). Comparing the J dependence of the two results above, we see that the first of these will dominate in the scaling limit $J \to 0$. Substituting $J \sim t^{-1/2}$ and normalizing, we end up with $\alpha_q = \alpha = \frac{1}{6}$, for $q < d + 4$. For the higher moments

($q > d+4$) we need to introduce the cut-off function F, so the integral will be dominated by the region $(x/t^{1/2}) \sim \mathrm{O}(1)$, where we can use the asymptotic power law from (89):

$$x^{(q)} \sim \frac{(\lambda t^{-1/2})^{-1}}{t^{-1/2}} \int_0^\infty \mathrm{d}x \frac{x^q}{x^{d+5}} F(x/t^{1/2}) \sim \lambda^{-1} t^{(q-2-d)/2}. \tag{112}$$

Consequently, we have the result $x^{(q)} \sim t^{\alpha_q}$, where (neglecting logarithmic corrections for $q = d+4$):

$$\alpha_q = \begin{cases} \dfrac{1}{6} & \text{for} \quad q < d+4 \\ \dfrac{1}{2} - \dfrac{d+2}{2q} & \text{for} \quad q > d+4. \end{cases} \tag{113}$$

In this case we have a discontinuity at $q = d+4$, a result of the power-law term being unimportant for $q < d+4$, but dominant for $q > d+4$. Once again we stress that the limiting behaviour $\alpha_q \to \frac{1}{2}$ as $q \to \infty$ is dependent on the diffusive form of the cut-off.

Thus, we predict the existence of multiscaling in the time-dependent case in qualitative agreement with Araujo *et al*, even though we are considering a different model. In general, power-law tails in the steady-state reaction front profiles should *always* lead to dynamic multiscaling, whatever their origin. These arguments are similar to those of Cornell *et al* [30], who find evidence for multiscaling in the reaction $nA + mB \to \emptyset$ with $(n, m) \neq (1, 1)$. However, in that case the solutions of the mean-field rate equations already give power laws, even without the addition of fluctuation effects.

Finally, we conclude that the available simulations are not directly applicable to our calculations of asymptotic power laws and multiscaling. However, if the asymptotics could be reached in a model with a finite reaction rate, our results should be amenable to numerical tests. These might be easiest in 1D where the power-law tail should be most pronounced.

Note added in proof. It has been pointed out by Cornell and Droz [31] that our choice of boundary conditions, with stochastic particle injection at a rate R on the system boundaries, leads to an extra source of noise. Explicit inclusion of this shot noise in the calculation would cause the fluctuations in the difference between the total number of A and B particles to grow without limit. However, in our calculation we have only considered noise arising from the classical reaction front, and have neglected the noise from the boundary conditions, which we believe to be unphysical.

Acknowledgments

The authors would like to thank B Lee for a reading of the manuscript. We also acknowledge financial support from the EPSRC.

Appendix A. Derivation of the Green function $G(\tilde{x}, \tilde{x}', \tilde{k}_\perp, \tilde{s})$

In this appendix we find a solution to (53) in the region $\tilde{x}' > 0$, and accurate for large $|\tilde{x}|$ i.e. when $|x| \gg (\bar{\lambda}\bar{J})^{-1/3}$):

$$G(\tilde{x}, \tilde{x}', \tilde{k}_\perp, \tilde{s}) = \begin{cases} \alpha \mathrm{Ai}[-\tilde{x} + \tilde{k}_\perp^2 + \tilde{s}] & \text{when} \quad \tilde{x} \leqslant 0 \\ \beta \mathrm{Ai}[\tilde{x} + \tilde{k}_\perp^2 + \tilde{s}] + \gamma \mathrm{Bi}[\tilde{x} + \tilde{k}_\perp^2 + \tilde{s}] & \text{when} \quad 0 \leqslant \tilde{x} \leqslant \tilde{x}' \\ \delta \mathrm{Ai}[\tilde{x} + \tilde{k}_\perp^2 + \tilde{s}] & \text{when} \quad \tilde{x} \geqslant \tilde{x}'. \end{cases} \tag{A1}$$

Considering the boundary conditions at $\tilde{x}'$ (continuity in G and a discontinuity in its derivative), we have

$$\beta \mathrm{Ai}(\tilde{x}' + \tilde{k}_\perp^2 + \tilde{s}) + \gamma \mathrm{Bi}(\tilde{x}' + \tilde{k}_\perp^2 + \tilde{s}) = \delta \mathrm{Ai}(\tilde{x}' + \tilde{k}_\perp^2 + \tilde{s}) \tag{A2}$$

$$\beta \mathrm{Ai}'(\tilde{x}' + \tilde{k}_\perp^2 + \tilde{s}) + \gamma \mathrm{Bi}'(\tilde{x}' + \tilde{k}_\perp^2 + \tilde{s}) - \delta \mathrm{Ai}'(\tilde{x}' + \tilde{k}_\perp^2 + \tilde{s}) = 1 . \tag{A3}$$

These equations can be solved for γ with the result that $\gamma = \pi \mathrm{Ai}(\tilde{x}' + \tilde{k}_\perp^2 + \tilde{s})$. The final boundary condition ($G \to 0$ as $\tilde{x} \to -\infty$) will (in principle) give a further relation between β and γ, as well as specifying α. But to use this condition we need to know the behaviour of G in regions near 0, where our asymptotic approximation breaks down. Consequently we must rely on numerical solutions, which reveal that for our purposes we may neglect the $\beta \mathrm{Ai}$ term in (A2). Solving for δ, we obtain

$$G(\tilde{x}, \tilde{x}', \tilde{k}_\perp^2, \tilde{s}) = \begin{cases} \pi \mathrm{Ai}(\tilde{x}' + \tilde{k}_\perp^2 + \tilde{s}) \mathrm{Bi}(\tilde{x} + \tilde{k}_\perp^2 + \tilde{s}) & \text{for} \quad 0 \ll \tilde{x} \leqslant \tilde{x}' \\ \pi \mathrm{Bi}(\tilde{x}' + \tilde{k}_\perp^2 + \tilde{s}) \mathrm{Ai}(\tilde{x} + \tilde{k}_\perp^2 + \tilde{s}) & \text{for} \quad \tilde{x} \geqslant \tilde{x}' \gg 0 . \end{cases} \tag{A4}$$

We can now use the asymptotic form of the Airy function [23] to simplify these expressions further:

$$\mathrm{Ai}(z) \sim \frac{1}{2\sqrt{\pi}} z^{-1/4} \mathrm{e}^{-(2/3)z^{3/2}} \qquad \mathrm{Bi}(z) \sim \frac{1}{\sqrt{\pi}} z^{-1/4} \mathrm{e}^{(2/3)z^{3/2}} . \tag{A5}$$

Hence, for $0 \ll \tilde{x} < \tilde{x}'$,

$$G = \tfrac{1}{2} (\tilde{x}' + \tilde{k}_\perp^2 + \tilde{s})^{-1/4} (\tilde{x} + \tilde{k}_\perp^2 + \tilde{s})^{-1/4} \mathrm{e}^{-\frac{2}{3}[(\tilde{x}' + \tilde{k}_\perp^2 + \tilde{s})^{3/2} - (\tilde{x} + \tilde{k}_\perp^2 + \tilde{s})^{3/2}]} \tag{A6}$$

with a similar expression for $\tilde{x} > \tilde{x}' \gg 0$. For $\tilde{x} \approx \tilde{x}' \gg 0$, we may expand the terms inside the exponential, to obtain

$$G_{\phi_1 \tilde{\phi}}(\tilde{x}, \tilde{x}', \tilde{k}_\perp, \tilde{s}) = \tfrac{1}{4} (\bar{\lambda} \bar{J})^{d/3} (\tilde{x} + \tilde{k}_\perp^2 + \tilde{s})^{-1/2} \mathrm{e}^{-(\tilde{x} + \tilde{k}_\perp^2 + \tilde{s})^{1/2} |\tilde{x} - \tilde{x}'|} . \tag{A7}$$

Appendix B. Evaluation of one-loop diagrams

The loop contained in the diagram in figure 7(*c*) is given by the integral

$$2\bar{\lambda}^{-1/3} \bar{J}^{2/3} (\bar{\lambda} \bar{J})^{d/3} \int \frac{\mathrm{e}^{-(\tilde{k}_\perp^2 + \mathrm{i}\tilde{s})^{1/2} |\tilde{x}_1''|}}{4(\tilde{k}_\perp^2 + \mathrm{i}\tilde{s})^{1/2}} \frac{\mathrm{e}^{-(\tilde{k}_\perp^2 - \mathrm{i}\tilde{s})^{1/2} |\tilde{x}_2''|}}{4(\tilde{k}_\perp^2 - \mathrm{i}\tilde{s})^{1/2}} \frac{\mathrm{e}^{-(\tilde{x}' + \tilde{k}_\perp^2 + \mathrm{i}\tilde{s})^{1/2} |\tilde{x}' - \tilde{x}_1''|}}{4(\tilde{x}' + \tilde{k}_\perp^2 + \mathrm{i}\tilde{s})^{1/2}}$$
$$\times \frac{\mathrm{e}^{-(\tilde{x}' + \tilde{k}_\perp^2 - \mathrm{i}\tilde{s})^{1/2} |\tilde{x}' - \tilde{x}_2''|}}{4(\tilde{x}' + \tilde{k}_\perp^2 - \mathrm{i}\tilde{s})^{1/2}} (2\tilde{x}_1'')(2\tilde{x}_2'') \, \mathrm{d}\tilde{x}_1'' \, \mathrm{d}\tilde{x}_2'' \frac{\mathrm{d}^{d-1}\tilde{k}_\perp \, \mathrm{d}\tilde{s}}{(2\pi)^d} \tag{B1}$$

where the prefactor of '2' counts the number of possible diagram configurations, and the s integration is along the real axis. In the integral we have used the form of the propagator for the ϕ field valid for $\tilde{x}_1'', \tilde{x}_2'', \tilde{x}' \gg 0$, and $\tilde{x}_1'', \tilde{x}_2'' \approx \tilde{x}'$, the region from which we expect the dominant contribution (as here the ϕ propagator falls off only as a power law). The $\tilde{x}_1''$ and $\tilde{x}_2''$ integrations are elementary, giving

$$2\bar{\lambda}^{-1/3} \bar{J}^{2/3} (\bar{\lambda} \bar{J})^{d/3} \tfrac{1}{16} \int \mathrm{e}^{-(\tilde{k}_\perp^2 + \mathrm{i}\tilde{s})^{1/2} \tilde{x}'} \mathrm{e}^{-(\tilde{k}_\perp^2 - \mathrm{i}\tilde{s})^{1/2} \tilde{x}'} \left[(\tilde{k}_\perp^2 + \mathrm{i}\tilde{s})^{-1/2} - \frac{2}{\tilde{x}'^2} \right]$$
$$\times \left[(\tilde{k}_\perp^2 - \mathrm{i}\tilde{s})^{-1/2} - \frac{2}{\tilde{x}'^2} \right] \frac{\mathrm{d}^{d-1}\tilde{k}_\perp \, \mathrm{d}\tilde{s}}{(2\pi)^d} . \tag{B2}$$

However, we notice that the leading $\tilde{x}'$ part of the integral is, in fact, a divergent power law. Furthermore, this divergence cannot be cancelled by the renormalization of the theory, as any such cancellation would have to arise from coupling constant renormalization at the tree level

(using (61)). As the renormalized tree-level result is still an exponential, cancellation with a power law cannot occur. Consequently, we must find another mechanism for the removal of the divergence, and this is provided by its cancellation with the divergent loop shown in figure 7(*b*). Turning now to the next to leading $\tilde{x}'$ term in the above integral, we have

$$-\bar{\lambda}^{-1/3}\bar{J}^{2/3}(\bar{\lambda}\bar{J})^{d/3}\frac{1}{4\tilde{x}'^{2}}\int \mathrm{e}^{-(\tilde{k}_\perp^2+\mathrm{i}\tilde{s})^{1/2}\tilde{x}'}\mathrm{e}^{-(\tilde{k}_\perp^2-\mathrm{i}\tilde{s})^{1/2}\tilde{x}'} \times\left[\frac{1}{(\tilde{k}_\perp^2+\mathrm{i}\tilde{s})^{1/2}}+\frac{1}{(\tilde{k}_\perp^2-\mathrm{i}\tilde{s})^{1/2}}\right]\frac{\mathrm{d}^{d-1}\tilde{k}_\perp\,\mathrm{d}\tilde{s}}{(2\pi)^d}\,. \tag{B3}$$

This can be rewritten as

$$\bar{\lambda}^{-1/3}\bar{J}^{2/3}(\bar{\lambda}\bar{J})^{d/3}\frac{2}{\tilde{x}'^{2}}\frac{\partial}{\partial\tilde{x}'}\int\frac{2\mathrm{e}^{-(\tilde{k}_\perp^2+\mathrm{i}\tilde{s})^{1/2}\tilde{x}'-(\tilde{k}_\perp^2-\mathrm{i}\tilde{s})^{1/2}\tilde{x}'}}{4(\tilde{k}_\perp^2+\mathrm{i}\tilde{s})^{1/2}4(\tilde{k}_\perp^2-\mathrm{i}\tilde{s})^{1/2}}\frac{\mathrm{d}^{d-1}\tilde{k}_\perp\,\mathrm{d}\tilde{s}}{(2\pi)^d} \tag{B4}$$

i.e. a constant times the derivative of the ψ propagator loop integral. Rewriting the ψ propagators entirely in momentum space, and performing a contour integration for $\tilde{s}$, we end up with

$$\bar{\lambda}^{-1/3}\bar{J}^{2/3}(\bar{\lambda}\bar{J})^{d/3}\frac{1}{\tilde{x}'^{2}}\frac{\partial}{\partial\tilde{x}'}\int\frac{\mathrm{e}^{\mathrm{i}\tilde{p}\tilde{x}'}}{\tilde{k}^2+(\tilde{p}-\tilde{k})^2}\frac{\mathrm{d}^d\tilde{k}\,\mathrm{d}\tilde{p}}{(2\pi)^{d+1}}\,. \tag{B5}$$

This integral may be done exactly using some standard results from [24], with the result

$$\bar{\lambda}^{-1/3}\bar{J}^{2/3}(\bar{\lambda}\bar{J})^{d/3}2^{-1-d}\pi^{-(d+1)/2}(1-d)\Gamma\left(\frac{d-1}{2}\right)\tilde{x}'^{-d-2}\,. \tag{B6}$$

To evaluate the contribution to $\langle\phi\rangle$ we now need to include the left most vertex and propagator:

$$-(\bar{\lambda}\bar{J})^{d/3}2^{-2-d}\pi^{-(d+1)/2}(1-d)\Gamma\left(\frac{d-1}{2}\right)\int\tilde{x}'^{-d-2}\tilde{x}^{-1/2}\mathrm{e}^{-\tilde{x}^{1/2}|\tilde{x}-\tilde{x}'|}\,\mathrm{d}\tilde{x}' \tag{B7}$$

giving the leading-order result

$$-(\bar{\lambda}\bar{J})^{-1}2^{-1-d}\pi^{-(d+1)/2}(1-d)\Gamma\left(\frac{d-1}{2}\right)x^{-d-3}\,. \tag{B8}$$

References

[1] Gálfi L and Rácz Z 1988 *Phys. Rev.* A **38** 3151
[2] Koo Y, Li L and Kopelman R 1990 *Mol. Cryst. Liq. Cryst.* **183** 187
[3] Jiang Z and Ebner C 1990 *Phys. Rev.* A **42** 7483
[4] Taitelbaum H, Havlin S, Kiefer J, Trus B and Weiss G 1991 *J. Stat. Phys.* **65** 873
[5] Koo Y and Kopelman R 1991 *J. Stat. Phys.* **65** 893
[6] Chopard B and Droz M 1991 *Europhys. Lett.* **15** 459
[7] Cornell S, Droz M and Chopard B 1991 *Phys. Rev.* A **44** 4826
[8] Araujo M, Havlin S, Larralde H and Stanley H E 1992 *Phys. Rev. Lett.* **68** 1791
[9] Ben-Naim E and Redner S 1992 *J. Phys. A: Math. Gen.* **25** L575
[10] Larralde H, Araujo M, Havlin S and Stanley H E 1992 *Phys. Rev.* A **46** 855
[11] Larralde H, Araujo M, Havlin S and Stanley H E 1992 *Phys. Rev.* A **46** R6121
[12] Cornell S, Droz M and Chopard B 1992 *Physica* **188A** 322
[13] Taitelbaum H, Koo Y, Havlin S, Kopelman R and Weiss G 1992 *Phys. Rev.* A **46** 2151
[14] Chopard B, Droz M, Karapiperis T and Rácz Z 1993 *Phys. Rev.* E **47** R40
[15] Cornell S and Droz M 1993 *Phys. Rev. Lett.* **70** 3824
[16] Droz M and Sasvári L 1993 *Phys. Rev.* E **48** R2343
[17] Araujo M, Larralde H, Havlin S and Stanley H E 1993 *Phys. Rev. Lett.* **71** 3592
[18] Cornell S 1994 *Preprint* UGVA/DPT 1994/10-857

[19] Lee B P 1994 *J. Phys. A: Math. Gen.* **27** 2633
[20] Lee B P 1994 Critical behaviour in non-equilibrium systems *PhD Thesis* University of California, Santa Barbara
Lee B P and Cardy J L 1994 *Preprint* OUTP-94-52S
[21] Doi M 1976 *J. Phys. A: Math. Gen.* **9** 1465, 1479
[22] Peliti L 1985 *J. Physique* **46** 1469
[23] Abramowitz M and Stegun I A 1965 *Handbook of Mathematical Functions* (New York: Dover)
[24] Gradshteyn I S and Ryzhik I M 1994 *Table of Integrals, Series, and Products* (San Diego: Academic)
[25] Hohenberg P C and Halperin B I 1977 *Rev. Mod. Phys.* **49** 435
[26] Bramson M and Lebowitz J L 1991 *J. Stat. Phys.* **65** 941
[27] Leyvraz F and Redner S 1991 *Phys. Rev. Lett.* **66** 2168; 1992 *Phys. Rev.* A **46** 3132
[28] Leyvraz F 1992 *J. Phys. A: Math. Gen.* **25** 3205
[29] Lee B P and Cardy J L 1994 *Phys. Rev.* E **50** R3287
[30] Cornell S, Koza Z and Droz M 1994 *Preprint* cond-mat/9412044
[31] Cornell S and Droz M 1995 Private communication